Marine Pollution Bulletin 165 (2021) 112094

Contents lists available at ScienceDirect

Marine Pollution Bulletin

journal homepage: www.elsevier.com/locate/marpolbul

Influence of seawater intrusion and heavy metals contamination on groundwater quality, Red Sea coast, Saudi Arabia

Fahad Alshehri [a], Sattam Almadani [a], Abdelbaset S. El-Sorogy [a,b,*], Essam Alwaqdani [c], Hussain J. Alfaifi [a], Talal Alharbi [a]

[a] Geology and Geophysics Department, College of Science, King Saud University, Saudi Arabia
[b] Geology Department, Faculty of Science, Zagazig University, Egypt
[c] Saudi Geological Survey, Jeddah 21514, Saudi Arabia

ARTICLE INFO

Keywords:
Seawater intrusion
Heavy metals contamination
Groundwater quality
Pollution indices
Multivariate statistics
Saudi Arabia

ABSTRACT

Groundwater samples were collected from 115 boreholes and dugwells to document the influence of seawater intrusion and heavy metals contamination on groundwater quality of the Al Qunfudhah region along the Red Sea coast, Saudi Arabia. The groundwater quality index (GWQI), metal index (MI), and heavy metal pollution index (HPI) were calculated and multivariate analyses were conducted. pH, EC, TDS, Cl^-, HCO_3^-, SO_4^{2-}, NO_3^-, NO_2^-, PO_4^{3-}, SiO_2, F^-, NH_4^+, Ca^{2+}, Mg^{2+}, Na^+, K^+, B, Ba, Cd, Cr, As, Ni, Pb, Se, Sb, Hg, Cu, and Zn were analyzed and interpreted. The average values for TDS, Ca^{2+}, Mg^{2+}, Na^+, K^+, Cl^-, HCO_3^-, SO_4^{2-}, B, and Se were greater than the permissible limit of WHO standards for drinking water. Piper plots indicated three types of groundwater facies, Na-K-SO_4-Cl (72.50%), Ca-Mg-So_4-Cl (25.50%), and Na-K-CO_3-HCO_3 (2%). Based on GWQI, MI, and HPI, approximately 37–70% of the groundwater samples fell under poor quality to unsuitable waters (strongly to severely affected), especially in the western part along the Red Sea coast. This proven the role of seawater intrusion through the NE–SW fault system, dissolution/precipitation of carbonates, silicates, fluorite, and gypsum, as well as anthropogenic factors in increasing the concentrations of heavy metals and controlling the chemistry and quality of the groundwater in the study area. These findings provide an important information on heavy metals pollution in coastal aquifer with seawater intrusion along the Red Sea.

1. Introduction

Rapid urbanization in developing countries has affected the availability and quality of groundwater because of overexploitation and improper waste disposal (Ramakrishnaiah et al., 2009; Panigrahy et al., 2015). Heavy metals are harmful to human health when their concentrations exceed permissible levels in drinking water (Prasanna et al., 2011). One of the natural sources of heavy metal contamination in groundwater is the weathering of rocks bearing minerals, while fertilizers from agricultural activities, sewage leachates, industrial wastes, and landfill leachates are possible anthropogenic sources (Rizwan et al., 2011; Evanko and Dzombak, 1997).

Groundwater is considered one of the most suitable sources to meet the increasing demand for fresh water for agricultural and tourist developments (Rezaei et al., 2019a, 2019b). The study area is located in the Tihamah plain along the Red Sea coast, southwest Saudi Arabia. It is bounded in the east by the Asir mountainous chain, which has the highest average rainfall in Saudi Arabia. The human population in the study area depends on the desalination of seawater and treatment of rainwater accumulated in dams for their drinking water (Sulaiman et al., 2018).

The basement rocks in the Al Qunfudhah area are exposed in the eastern region and dip westward beneath the sedimentary cover to depths of up to 2200 m along the coast (Sulaiman et al., 2018). Two fault systems are recognized that follow the NNW–SSE and NE–SW directions. Some of the Miocene northwest-trending faults were intruded by gabbro and basaltic lavas flowed from fissures (Prinz, 1984; Abdelkareem et al., 2020). Remote sensing has identified shallow groundwater in the study area and fold systems trending in the N—S, NNE–SSW, and NNW–SSE directions, reflecting the E–W compressional regime and Cenozoic normal faults relating to Red Sea rifting (Alshehri et al., 2020; Abdelkareem et al., 2020).

Many published works have investigated the groundwater quality index (GWQI) around the world, heavy metal pollution index (HPI), and

* Corresponding author at: Geology and Geophysics Department, College of Science, King Saud University, Saudi Arabia.
E-mail addresses: elsorogyabd@yahoo.com, asmohamed@ksu.edu.sa (A.S. El-Sorogy).

https://doi.org/10.1016/j.marpolbul.2021.112094
Received 24 December 2020; Received in revised form 21 January 2021; Accepted 22 January 2021
Available online 24 February 2021

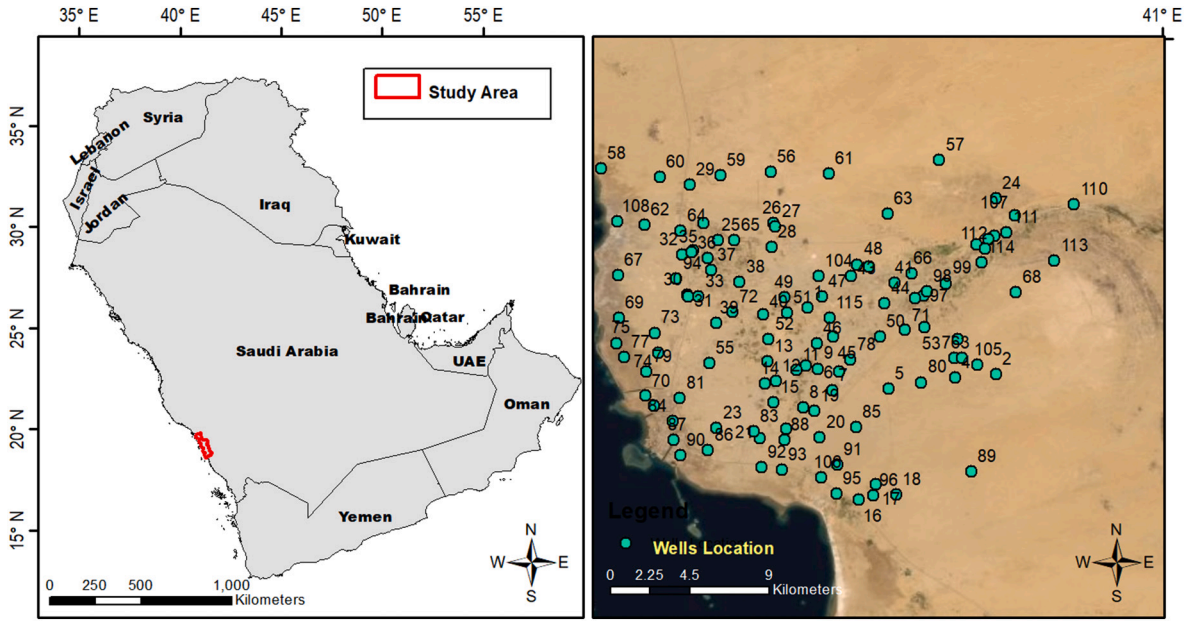

Fig. 1. Location map of the groundwater samples, Al Qunfudhah area, Saudi Arabia.

metal index (MI) for groundwater quality (e.g., Mohan et al., 1996; Backman et al., 1997; Sahu and Sikdar, 2008; Prasad and Sangita, 2008; Vasanthavigar et al., 2010; Rizwan et al., 2011; Sheykhi and Moore, 2012; Nabizadeh et al., 2013; Sirajudeen et al., 2014; Bodrud-Dozaa et al., 2016; Rezaei et al., 2019a; Chiamsathit et al., 2020). Therefore, this study aimed to document the influence of seawater intrusion and heavy metals contamination on groundwater quality in Al Qunfudhah region, Red Sea coast, Saudi Arabia (Fig. 1) using hydrogeochemical characteristics groundwater quality index (GWQI), metal index (MI), heavy metal pollution index (HPI), and multivariate analyses.

2. Geology and hydrogeology

The study area is bounded to the east by the Asir mountainous chain, which runs parallel to the Red Sea and is composed largely of Proterozoic volcanic-sedimentary rock units of the Arabian Shield. The older rocks were folded and intruded by plutonic and hypabyssal intrusive tonalite and diorite batholiths, following the diapiric intrusion of monzogranite to granodiorite, and accompanied by regional metamorphism to greenschist-amphibolite facies (Sulaiman et al., 2018). The volcanic-sedimentary rock units of the Arabian Shield are unconformably overlain by thick sedimentary sequences, ranging in age from the Cambrian to recent times (Sultan et al., 1990; Prinz, 1983; Abdelkareem et al., 2020; Alshehri et al., 2020).

The Asir mountainous region receives the highest average annual precipitation in Saudi Arabia (Sulaiman et al., 2018; Alshehri et al., 2020). The Tihamah plain is covered by Quaternary sediments, wadi deposits, and eolian sediments, which can reserve precipitated rainfall and flash flood water (Abdelkareem et al., 2020). Topographically, Al Qunfudhah Province descends in height from a maximum altitude of about 1000 m in the east and declines steeply to the west (Sulaiman et al., 2018). It is built along one of the primary channels draining a large watershed, making it a popular site for organized agricultural development (Bayumi et al., 2000; Sahour et al., 2020a; Alshehri et al., 2020).

Rainwater flows from Asir mountainous ridges to the low land at the coastal plain, where a considerable amount of the runoff water penetrates through the sedimentary cover and accumulates in the basin areas of the basement surface (Sulaiman et al., 2018). Abdelkareem et al. (2020) concluded that the interaction between fault systems formed a set of closed elongated basins, which are considered potential regions for groundwater accumulation in the study area, and the N—S fault escarpments represent basin boundaries for all the wadis that run from east to the west. The 2 m rise in groundwater in the study area over the last three years has been attributed by Alshehri et al. (2020) to increased precipitation in the last three years compared with previous years.

3. Material and methods

Hydrochemical data for the western coastal plain of Saudi Arabia were obtained from reports from the Saudi Ministry of Water and Electricity. A total of 115 groundwater samples were collected, which were mostly from boreholes, with a few from dugwells (Fig. 1). The analyzed indices include pH, EC, TDS, NO_3^-, NO_2^-, NH_4^+, PO_4^{-3}, F^-, SO_2, major ions (Ca^{2+}, Mg^{2+}, Na^+, K^+, Cl^-, HCO_3^-, SO_4^{2-}), and heavy metals (Hg, Sb, Cu, Cr, B, Ba, Pb, Ni, Se, Cd, As, Zn). A Piper plot was prepared to determine the groundwater facies. The GWQI, HPI, and MI were used to evaluate groundwater quality. The procedures and calculation methods of these indices and their categories are presented in Table 1. The coordinates of the groundwater bore holes (samples), hydrogeochemical parameters, major anions, major cations, heavy metals, and pollution indices are presented in supplementary Table 1. Principal component analysis, Pearson's correlation coefficients, and hierarchical clustering analysis were used as statistical analyses using SPSS software to identify the possible sources of HMs in the investigated groundwater. Maps and plots were prepared using ArcGIS 10.5, Surfer 12.0, Aquachem 4.0, and Microsoft Excel 2010.

4. Results and discussion

4.1. Hydrogeochemical characteristics

The TDS values ranged from 516 in sample 2 to 138,182 in sample 82, with a mean of 12,968 mg/l (Table 2). Ten samples (8.7%) were classified as freshwater (TDS ‹1000 mg/l), 75 samples (65.22%) were classified as brackish (1000 < TDS < 10,000), and the remaining 30 samples (26.09%) were classified as saline (TDS > 10,000). The samples with a higher TDS (e.g., samples 58, 61, 62, 66, 69–75, 79–82, 86, 87, 90, and 92.) are located in the western part of the study area, along the Red Sea coast (Fig. 2). The bulk of the major cationic concentration

Table 1
Procedures, calculation methods, and categories of the groundwater quality index (GWQI), heavy metal pollution index (HPI), and metal index (MI).

Indices	Procedures of calculation and classifications
Metal index (MI)	$MI = \sum_{i=1}^{n} \frac{Ci}{Mac}$ where MI is the metal index, C is the concentration of each element in the solution, MAC is the maximum allowed concentration of each element, and the subscript i indicating the ith sample. According to Lyulko et al. (2001); Caerio et al. (2005); Tamasi and Cini (2004); Rezaei et al. (2017), MI is classified into six categories: MI < 0.3 Very pure; MI = 0.3–1.0 Pure; MI = 1.0–2.0 Slightly affected; MI = 2.0–4.0 Moderately affected; MI = 4.0–6.0 Strongly affected; MI > 6.0 Seriously affected
Heavy metal pollution index (HPI)	$HPI = \frac{\sum W_i Q_i}{\sum W_i}$ where, Q_i is the sub-index of the ith parameter and W_i is the unit weight for the ith parameter. $Q_i = \Sigma\left(\frac{[M_i(-)L_i]}{S_i - L_i}\right)$ where M_i, I_i and S_i are the monitored heavy metal, ideal and standard values of the ith parameter, respectively. The sign (−) indicates numerical difference of the two values, ignoring the algebraic sign. Groundwater water quality is classified into three categories based on modified heavy metal pollution index (Mohan et al., 1996; Bodrud-Dozaa et al., 2016) HPI < 45 Low pollution; HPI = 45–90 Medium pollution; HPI > 90 High pollution
Groundwater quality index (GWQI)	$WQI = \Sigma Q_n W_n / \Sigma W_n$ $Q_n = 100[V_n - V_{in}]/[S_n - V_{in}]$ $W_n = K/S_n$ where, Q_n is the quality rating for nth water quality parameter; V_n is the estimated value of nth parameter in given sampling station; Sn is the standard permissible value of the nth parameter; V_{in} is the ideal value of nth parameter in pure water; W_n is the unit weight for nth parameter; K is a constant for proportionality. Groundwater water quality is classified into three categories based on modified GWQI (Vasanthavigar et al., 2010; Sharma and Patel, 2010) GWQI <50 Excellent water; GWQI = 50–100 Good water; GWQI = 100.1–200 Poor water; GWQI = 200.1–300 Very poor water; GWQI >300 Water unsuitable for drinking purposes

Table 2
The minimum, maximum, average, standard deviation, and maximum allowable concentrations (MAC) of the measured physical and chemical parameters, and the pollution indices.

	Minimum	Maximum	Mean	Std. dev.	MAC
pH	6.8	8.1	7.5	0.25	NA
EC	791	172,000	19,044	32,132.57	NA
TDS (mg/l)	516	138,182	12,968	24,164.43	1000
Ca^{2+} (mg/l)	11.30	2204.95	374.18	400.95	75
Mg^{2+} (mg/l)	8.63	2893.40	322.16	517.15	30
Na^{+} (mg/l)	49.00	47,582.00	3906.60	8260.58	200
K^{+} (mg/l)	0.01	2766.79	220.11	462.44	12
NH_4^{+} (mg/l)	0.03	1.59	0.13	0.24	NA
Cl^{-} (mg/l)	30.00	80,051.00	6729.06	14,167.28	250
HCO_3^{-} (mg/l)	83.00	609.00	251.59	107.25	200
NO_3^{-} (mg/l)	0.01	106.00	22.64	24.15	50
SO_4^{2-} (mg/l)	1.82	5250.00	1138.24	1023.94	250
NO_2^{-} (mg/l)	0.00	1.19	0.07	0.18	3
PO_4^{3-} (mg/l)	0.01	0.01	0.01	0.00	NA
F^{-} (mg/l)	0.27	3.30	1.30	0.77	1.5
SiO_2 (mg/l)	10.85	126.90	43.23	17.99	NA
As (μg/l)	0.10	69.66	4.00	8.62	10
B (μg/l)	155	49,300	2434	5043	2400
Ba (μg/l)	1.87	464.11	29.85	57.83	700
Cd (μg/l)	0.01	3.34	0.16	0.33	3
Cr (μg/l)	0.09	10.58	1.27	1.89	50
Cu (μg/l)	0.05	63.68	7.69	16.09	2000
Hg (μg/l)	0.02	72.62	2.04	9.12	6
Ni (μg/l)	0.67	234.16	25.62	30.55	70
Pb (μg/l)	0.09	434.57	7.11	42.79	10
Sb (μg/l)	0.49	23.60	1.12	2.68	20
Se (μg/l)	0.32	1202.93	86.58	154.77	40
Zn (μg/l)	0.09	690.18	57.90	123.19	50
MI	0.79	66.35	5.89	8.45	
HPI	22.19	1493.63	180.23	268.12	
GWQI	22.90	5044.88	503.62	899.21	

MAC, maximum allowable concentration.

comprises of Na^{+} (mean 3906.60 mg/l), followed by Ca^{2+} (374.18 mg/l), Mg^{2+} (322.16 mg/l), and K^{+} (220.11 mg/l). The major anions are dominated by Cl^{-} (6729.06 mg/l), followed by SO_4^{2-} (1138.24 mg/l), HCO_3^{-} (251.59 mg/l), NO_3^{-} (22.64 mg/l), F^{-} (1.30 μg/l), NO_2^{-} (0.07 mg/l), and PO_4^{-3} (0.01 mg/l). The average values of TDS, Ca^{2+}, Mg^{2+}, Na^{+}, K^{+}, Cl^{-}, HCO_3^{-}, and SO_4^{2-} were greater than the permissible limit of WHO standards for drinking water (Table 2). Fluoride was derived to the groundwater from industrial effluents, phosphatic fertilizers, continental dust, and leaching of the rocks rich in fluorine (Aswathanarayana et al., 1985; Dissanayake and Chandrajith, 2009).

On the cationic triangle, 75% of the samples were categorized as $Na^{+} + K^{+}$ dominant, 23.85% had no dominant type, and 1.15% was categorized as Ca dominant (Fig. 3). On the anionic triangle, 75% of the groundwater samples were categorized as Cl^{-} dominant, 23.70% had no dominant type, 1.15% was categorized as SO_4 dominant, and 1.15% was categorized as HCO_3^{-} dominant. $Na^{+} + K^{+}$ and Cl^{-} were the most dominant ions, and based on their dominance, the groundwater facies were classified into three types (Fig. 4): Na-K-SO_4-Cl (72.50%), Ca-Mg-So_4-Cl (25.50%), and Na-K-CO_3-HCO_3 (2%), indicating seawater intrusion, gypsum, and halite dissolution, some reverse ion exchange, and anthropogenic influences (Kumar, 2014).

4.2. Heavy metals concentration and distribution

The concentration of heavy metals in groundwater samples was compared with heavy metal MACs from WHO (2004, 2011). B was the most abundant heavy metals (2434 μg/l), followed by Se (86.58 μg/l), Zn (57.90 μg/l), Ba (29.85 μg/l), Ni (25.62 μg/l), Cu (7.69 μg/l), Pb (7.11 μg/l), As (4.00 μg/l), Hg (2.04 μg/l), Cr (1.27 μg/l), and Sb (1.12 μg/l). The mean values of B and Se were greater than the permissible limit of WHO standards for drinking water (Table 2). Arsenic levels ranged from 0.10 to 69.66 μg/l and were higher than the acceptable WHO standards in 13 well samples (58, 60, 62, 66, 69, 70, 74, 75, 77, 82, 83, 86, and 87).

Zinc values ranged from 0.09 to 690.18 μg/l (Table 2). The Zn values were higher than the WHO standards (50 μg/l) in 26 well samples (57, 58, 60, 61, 63, 66, 68–71, 73–75, 77, 78, 80–82, 84–87, 89–91, and 96). Nickel values ranged from 0.67 to 234.16 μg/l. The Ni concentration was higher than the corresponding WHO values (70 μg/l) in nine well samples (23, 24, 53, 58, 60, 63, 73, 82, and 89). The Pb concentrations ranged from 0.09 to 434.57 μg/l, which were higher than the corresponding WHO values (10 μg/l) at in seven well samples (59, 61, 68, 71,

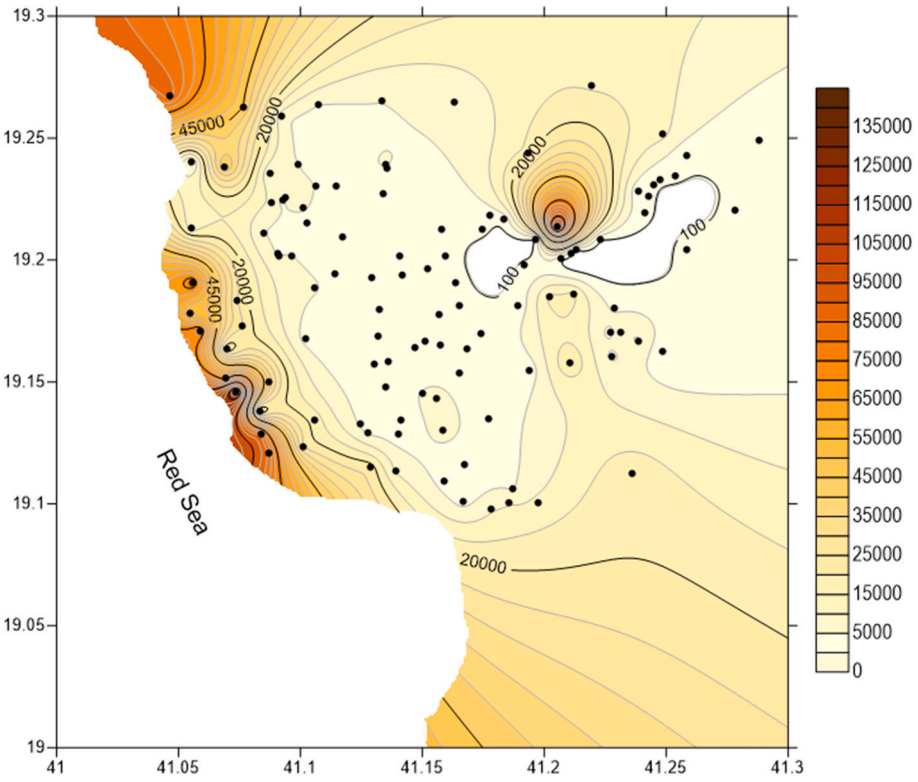

Fig. 2. TDS distribution map of the study area. All values are in mg/l.

78, 80, and 85).

Mercury values ranged from 0.02 to 72.62 μg/l and were higher than the WHO standard (6 μg/l) at in six well samples (56, 57, 64, 65, 72, and 91). Fluoride values ranged from 0.27 to 3.30 μg/l, which was higher than the WHO standard (1.5 μg/l) at 42 wells (36.52% of the total samples). Boron values ranged from 155.13 to 49,299.89 μg/l and were higher than the corresponding WHO values (2400 μg/l) at 33 wells (28.70%). Selenium values ranged from 0.32 to 1202.93 μg/l. The Se concentration was higher than the corresponding WHO values (40 μg/l) at 45 wells (39.13%). Antimony and cadmium values were lower than the corresponding WHO values (20 and 3 μg/l, respectively) at all the investigated wells, except well 75 (Sb) and well 73 (Cd). Cd had a positive correlation with As, B, and Ba. Barium, chromium, and cupper values were less than their acceptable WHO values of 700, 50 and 2000

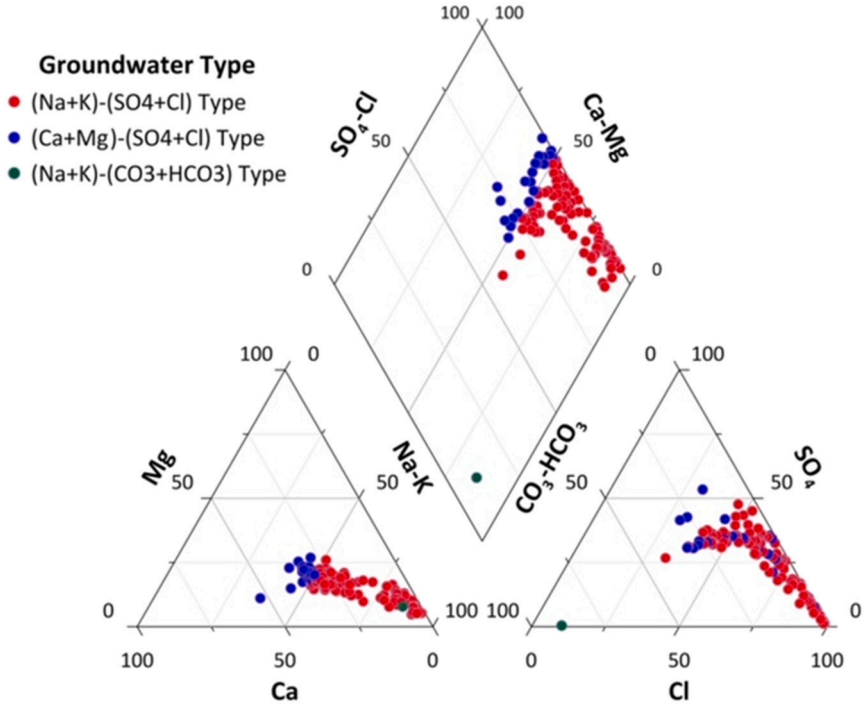

Fig. 3. Classification of the groundwater facies using a Piper diagram.

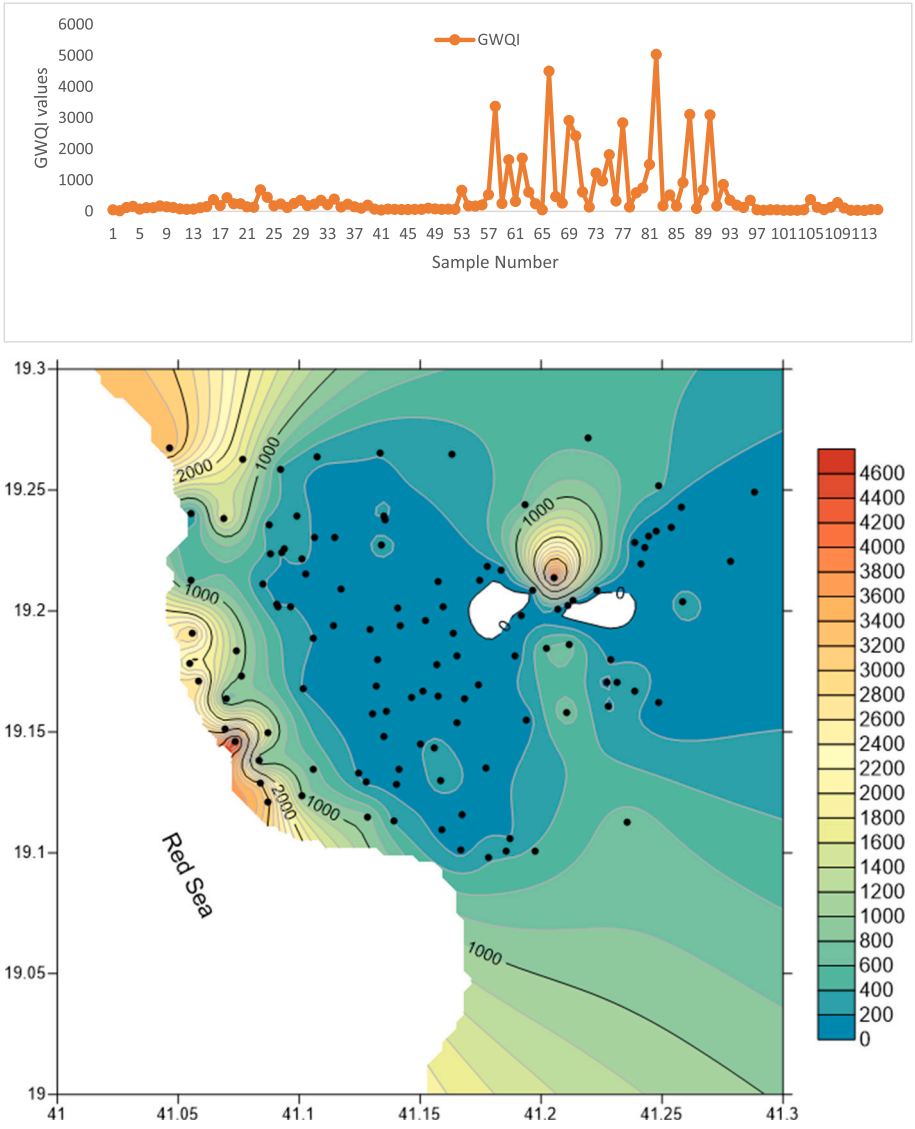

Fig. 4. GWQI distribution chart and map in the study area.

µg/l, respectively.

4.3. Pollution indices

The GWQI reflects the composite influence of the different water quality parameters on the suitability of water for drinking purposes (Sahu and Sikdar, 2008). It provides the composite influence of individual water quality parameters on the overall quality of water for human consumption (Bodrud-Dozaa et al., 2016). GWQI values ranged from 22.90 in sample 2 to 5044.88 in sample 82 (Supplementary Table 1, Fig. 4). Twelve samples (10.43%) were classified as having excellent water quality (GWI ˂ 50). The excellent quality water samples (2, 41, 97–103, 111–113) were from the eastern part of the study area and have the lowest levels of TDS, EC, Ca^{2+}, Mg^{2+}, Na^{+}, Cl^{-}, $SO4^{2-}$, B, Ba, Cd, Ni, Se, Hg, Pb, Sb, and MI. Twenty-two samples (19.13%) were classified as good quality water (GWQI = 50–100), and they were from the middle and eastern parts of the study area (e.g., 1, 5, 11–13, 42–47, 49–52, 114, and 115). Thirty-one samples (26.96%) were classified as poor quality water (GWQI = 100.1–200), and they were mostly from the eastern part (e.g., 6–10, 14, 15, 54, 55, 72, and 78). Thirteen samples (11.30%) were classified as very poor quality water (GWQI = 200.1–300), and the remaining 36 samples (31.30%) are categorized as water unsuitable for drinking purposes (GWQI >300). Most of the very poor and unsuitable samples for drinking purposes were from the western part of the study area along the Red Sea coast (e.g., 16, 18, 64, 67, 69–71, 73–77, 79–82, 92, and 93), and they had the highest values of the investigated anions, cations, and the heavy metals, except Hg, Pb, and Cr.

The MI helps to quickly evaluate the overall quality of drinking water, and it takes into account the possible additive effects of heavy metals on human health (Enaam Abdullah, 2013; Rezaei et al., 2017). MI values ranged from 0.79 in sample 98 to 66.35 in sample 73 (Supplementary Table 1, Fig. 5). Three wells (samples 41, 98, and 101) were categorized as pure water (MI = 0.3–1.0), and they were from the western part of the study area. Thirty-four samples (29.57%) were slightly affected (MI = 1.0–2.0), and they were mostly from the eastern and central parts. Thirty-six samples (31.30%) were categorized as moderately affected (MI = 2.0–4.0), and they were mostly from the central part. Twelve samples (10.43%) were categorized as strongly affected (MI = 4.0–6.0), and the remaining 30 samples (26.09%) were categorized as severely affected (MI > 6.0). The strongly and severely affected groundwater samples (e.g., 23, 58, 62, 67, 69, 82, 89, 90, 93, and 106) were from the western part of the study area close to the coast, and they had the highest values of the investigated anions cations, (except NO_2), and the heavy metals (except Cr).

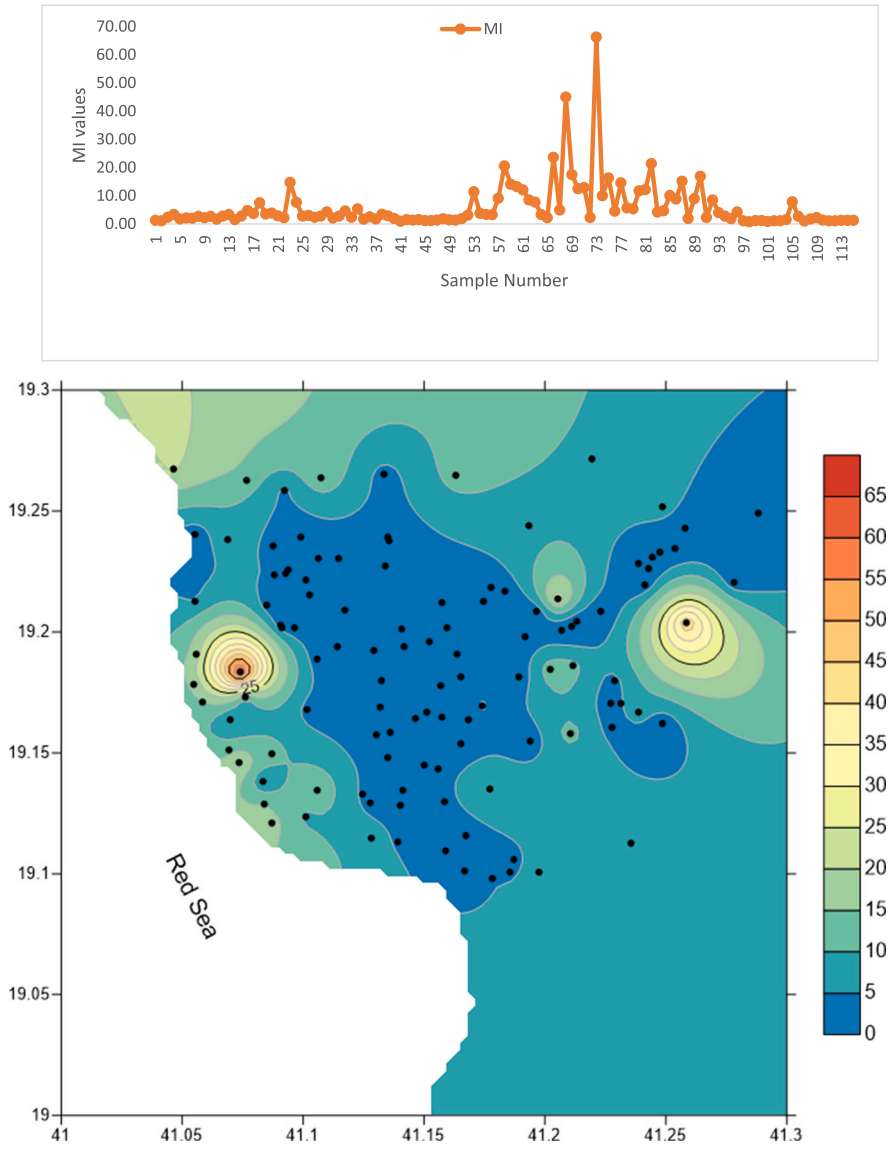

Fig. 5. MI distribution chart and map in the study area.

Sirajudeen et al. (2014) identified HPI as a quantity reflecting the composite influence of different dissolved heavy metals. It is a powerful tool for ranking the amalgamated effects of individual heavy metals on overall water quality (Rizwan et al., 2011; Rezaei et al., 2017). HPI values ranged from 22.19 in sample 42 to 1493.63 in sample 66 (Supplementary Table 1, Fig. 6). Thirty-four samples (29.57%) were classified as having low levels of pollution (HPI < 45), and they were mostly from the eastern and central parts of the study area. Twenty-two samples (19.13%) were classified as having medium levels of pollution (HPI = 45–90), and the remaining 59 samples (51.30%) are categorized as having high levels of pollution (HPI > 90).

4.4. Possible sources of ions and heavy metals

Hierarchical cluster analysis (HCA) and principal component analysis (PCA) are two useful tools to understand the sources and influencing factors of groundwater chemistry (Wu, 2020). Q mode HCA categorized the 115 groundwater samples into two strongly unequal clusters, have distinctive hydrochemical characteristics (Supplementary Fig. 1). The smaller cluster includes samples 66 and 82, which account the highest values of TDS, EC, Mg^{2+}, Na^{+}, K^{+}, Cl^{-}, F^{-}, Zn, HPI, and GWQI. The larger cluster consists of four groups showing strong hydrochemical similarities, and are controlled by similar factors with similar degree of influence (Cloutier et al., 2008; Sahour et al., 2020b). The smallest group includes the severely affected sample 73, which had the highest values of As, B, Ba, Cd, Ni, Se, and MI. The second group includes samples 58, 69, 77, 87, and 90, which had the highest values of Mg^{2+} and SO_4^{2-}, Al, Cu, and Sb. The third group accounts samples 60, 62, 70, 75, and 81, which had the highest Cu and Sb values. The fourth group includes the remaining groundwater samples and had the lowest values for anions, cations and heavy metals, except for Pb (sample 68), Cr (sample 13), NO_2^- (sample 54), HCO_3^- (sample 67), SiO_2 (Sample 23), Ca^{2+} (sample 89), and NO_3^- (Sample 53). R mode HCA classified the hydrogeochemical parameters into two unequal clusters (Fig. 7). The smaller cluster includes TDS and EC, while the larger one includes the remaining hydrogeochemical parameters and pollution indices.

The correlation coefficient matrix (Table 3) revealed a significant correlation between TDS and EC, Ca^{2+}, Mg^{2+}, Na^{+}, K^{+}, NH_4^{+}, Cl^{-}, and SO_4^{2-} (r = 0.995, 0.533, 0.888, 0.996, 0.957, 0.559, 0.998, and 0.672, respectively), as well as between SO_4^{2-} and EC, Ca^{2+}, Mg^{2+}, Na^{+}, K^{+}, NH_4^{+}, and Cl^{-}(r = 0.678, 0.505, 0.622, 0.664, 0.545, 0.576, and 0.633, respectively), implying a common source of these ions (Alfaifi et al., 2021), and suggesting the possible source of Ca^{2+} and SO_4^{2-} is the dissolution of gypsum in sabkhas (Li et al., 2016; Wu et al., 2020). Also,

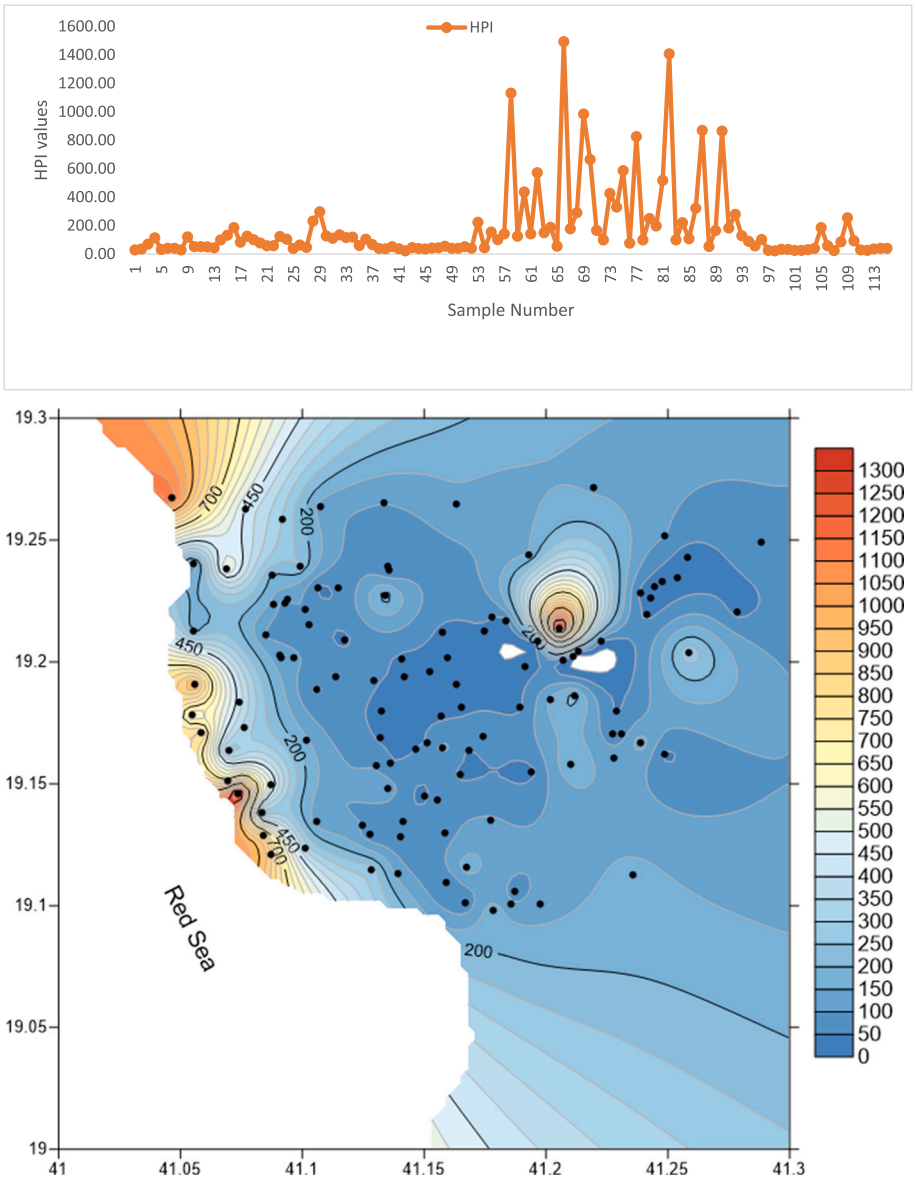

Fig. 6. HPI distribution chart and map in the study area.

the correlation matrix revealed a strong correlation between Zn and F, B, Cu, and Se; and between Ni and F^-, As, B, Ba, and Cd. NO_2^- and NO_3^- are negatively correlated with the ramming cations and anions, indicating a different source. More than 50% of the samples have NO_3^- values that were much higher than 10 mg/l, which could be attributed to extensive agricultural activities, especially in the central part of the study area (Abu Jabal et al., 2014). The groundwater quality index (GWQI) showed a strong positive correlation with EC, Ca^{2+}, Mg^{2+}, Na^+, K^+, $NH4^+$, Cl^-, $SO4^{2-}$, F^-, TDS, Cu, Zn, MI, HPI, and Se. Moreover, the metal index (MI) is strongly correlated with As, B, Ba, Cd, Cu, Ni, Se, and Zn, while the heavy metal pollution index (HPI) is strongly correlated with Cu, Se, and Zn.

PCA generates seven principal components that account for 45.00%, 11.49%, 8.06%, 5.26%, 4.62%, 4.09%, and 3.64%, respectively, and cumulatively explain 82.17% of the total variance (Table 4). The first component shows strong association with EC, Mg^{2+}, Na^+, K^+, NH_4^+, Cl^-, SO_4^{2-}, F^-, TDS, Cu, Se, HPI, and GWQI, reflecting the salinity component and probably shows the result of mineral water reactions in the study area (Rezaei et al., 2017). The natural processes responsible for these strong associations are mainly the dissolution/precipitation of carbonates, silicates, fluorite, and gypsum. The higher values of Cl^-, especially in samples located along the coastal area could be attributed to saline water intrusion and the presence of sabkhas (Baghvand et al., 2010; Singaraja et al., 2014). The finding that the Na^+ values in most samples were higher than the WHO standards could be a result of ion exchange reactions or silicate weathering (Li et al., 2016).

The second component had high loadings for As, B, Ba, Cd, Ni, Sb, Se, and MI, which represents mixed natural and anthropogenic process. These elements might originate from the seepage of agricultural activities, intensive weathering and leaching by rock-water interactions (Li et al., 2018; Rahman et al., 2014). Higher concentrations of As could be attributed to weathering and erosion of As-bearing minerals and using arsenical pesticides in the study area (Wang and Mulligan, 2006a, 2006b; Naidu and Bhattacharya, 2009; Rezaei et al., 2017). Moreover, the second component indicates the role of salinity and seawater intrusion in increasing the aqueous concentrations of some heavy metals in soil-groundwater systems (Lu et al., 2004; Basahi et al., 2018; Kampouroglou and Economou-Eliopoulos, 2017; Wen et al., 2019).

The third component had high loading of pH and HCO_3^-. The fourth, fifth, sixth, and seventh components had high loading of (SO_4^{2-}), (PO_4^{3-}),

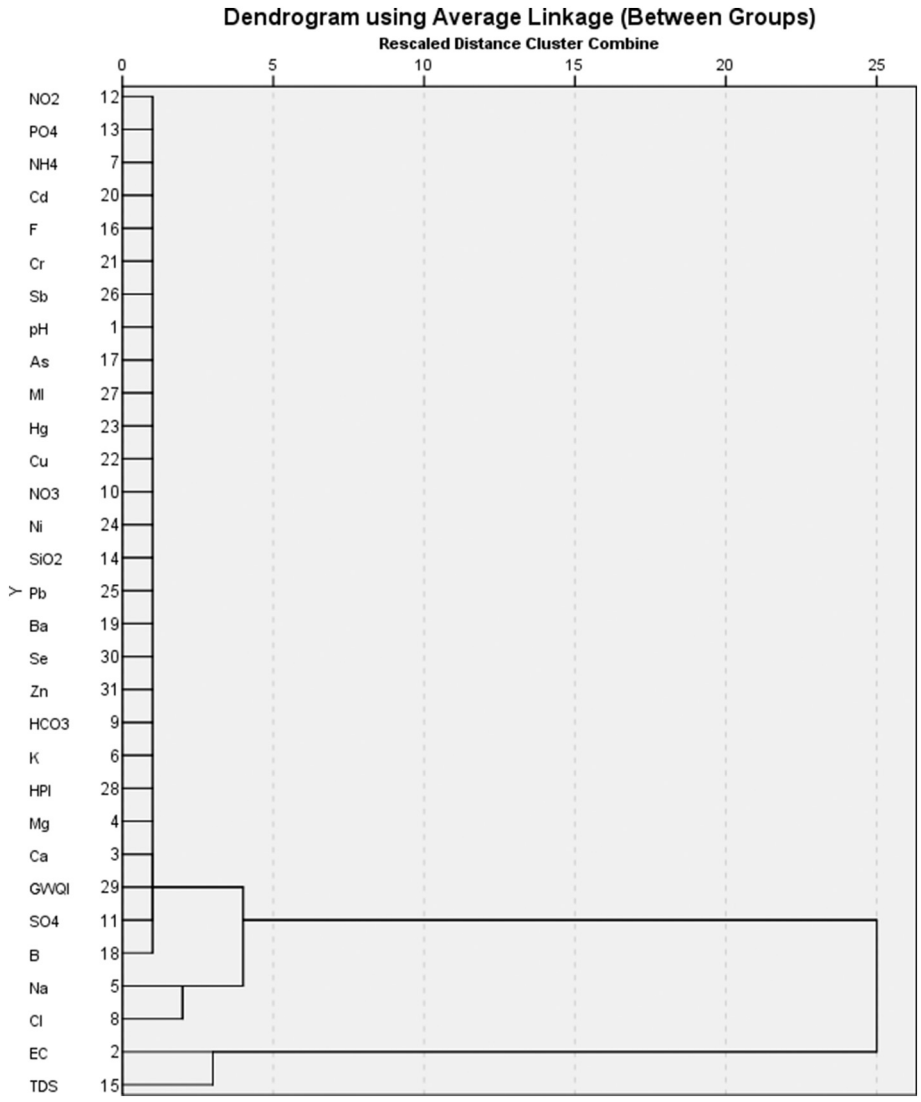

Fig. 7. R mode HCA of the hydrogeochemical parameters in groundwater samples.

(Pb, Zn, and MI), and (Hg), respectively, which was attributed to the excessive use of phosphate and zinc sulfate in fertilizers and pesticides in agricultural activities (Alfaifi et al., 2021; Rezaei et al., 2019a, 2019b). The heavily polluted samples (e.g. 57–64, 66–75, 77–87, 89–93) are located close to the Red Sea coast and were characterized by the highest values of anions, cations, and heavy metals, suggesting the significant role of seawater intrusion in increasing the concentrations of heavy metals in groundwater (Wen et al., 2019; Basahi et al., 2018; Kampouroglou and Economou-Eliopoulos, 2017). This is supported by the NE–SW fault system that expected to act as pathways for seawater intrusion into the groundwater and for groundwater discharge to the Red Sea (Sulaiman et al., 2018).

5. Conclusions

The present study documented the influence of seawater intrusion and heavy metals contamination on groundwater quality of Al Qunfudhah region, Red Sea coast, Saudi Arabia, using groundwater quality index (GWQI), degree of contamination (C_d), heavy metal pollution index (HPI), and multivariate statistical techniques. The following findings have been obtained.

1. The average values of TDS, Ca^{2+}, Mg^{2+}, Na^{+}, K^{+}, Cl^{-}, HCO_3^{-}, SO_4^{2-}, B, and Se were greater than the permissible limit of the WHO standards for drinking water. The high NO_3^{-} and SO_4^{2-} values, especially in the central part of the study area, could be attributed to the excessive use of fertilizers and pesticides in the agriculture. The high values of Cl^{-}, especially in samples from along the coastal area could be attributed to saline water intrusion and the presence of sabkhas.
2. Na + K and Cl were found to be the major ions contributing to the bulk of the TDS, which ranged from 516 in the central part of the study area to 138,182 mg/l in the western part of the study area, along the Red Sea coast. Piper plots showed three types of groundwater facies in the study area: Na-K-SO_4-Cl (72.50%), Ca-Mg-So_4-Cl (25.50%), and Na-K-CO_3-HCO_3 (2%).
3. GWQI values categorized the groundwater samples as 10.43% excellent quality, 19.13% good quality, 26.96% poor quality, 11.30% very poor quality, and 31.30% water unsuitable for drinking purposes. The MI and HPI values coincided to a great extent with the GWQI values. Most of the very poor and unsuitable for drinking waters (the highly polluted samples) were collected from the western part of the study area, along the Red Sea coast.
4. Seawater intrusion, dissolution/precipitation of carbonates, gypsum, halite, fluorite, silicates, and agricultural activities are the primary factors influencing groundwater chemistry and quality in the study

Table 3
Correlation coefficient for the analyzed parameters.

	pH	EC	Ca	Mg	Na	K	NH_4	Cl	HCO_3	NO_3	SO_4	NO_2	PO_4	SiO_2	TDS	F	As	B	Ba	Cd	Cr	Cu	Hg	Ni	Pb	Sb	MI	HPI	GWQI	Se	Zn
pH	1																														
EC	-.004	1																													
Ca^{2+}	-.279**	**.559****	1																												
Mg^{2+}	-.090	**.905****	**.703****	1																											
Na^{+}	.023	**.987****	.469**	**.857****	1																										
K^{+}	.013	**.950****	.392**	**.818****	**.956****	1																									
$NH4^{+}$	-.012	**.578****	.376**	.496**	**.555****	.497**	1																								
Cl^{-}	-.009	**.993****	**.533****	**.888****	**.993****	**.962****	**.545****	1																							
HCO_3^{-}	.455**	.337**	-.171	.254**	.351**	.321**	.206*	.301**	1																						
NO_3^{-}	-.413**	-.168	-.149	-.194*	-.153	-.089	-.209*	-.137	-.377**	1																					
SO_4^{2-}	-.007	**.678****	**.505****	**.622****	**.664****	**.545****	**.576****	**.633****	.272**	-.331**	1																				
NO_2^{-}	-.129	-.148	-.175	-.157	-.129	-.113	-.125	-.132	-.095	.274**	-.188*	1																			
PO_4^{3-}	.296**	.161	.054	.130	.161	.176	.116	.157	.216*	-.391**	.068	-.453**	1																		
SiO_2	-.313**	-.508**	-.242**	-.443**	-.499**	-.472**	-.234*	-.490**	-.328**	.293**	-.313**	.075	-.312**	1																	
TDS	-.008	**.995****	**.533****	**.888****	**.996****	**.957****	**.559****	**.998****	.316**	-.152	**.672****	-.139	.159	-.493**	1																
F	.064	**.691****	**.511****	**.609****	**.651****	**.563****	**.520****	**.646****	.281**	-.305**	**.645****	-.132	.071	-.554**	**.661****	1															
As	.122	**.502****	.162	.426**	.476**	.438**	.252**	.462**	.410**	-.202*	.248**	-.100	.151	-.427**	.464**	.471**	1														
B	.041	.420**	.272**	.385**	.380**	.325**	.258**	.374**	.347**	-.185*	.368**	-.111	.083	-.303**	.383**	.474**	**.794****	1													
Ba	-.008	.436**	.427**	**.515****	.385**	.370**	.207*	.414**	.237*	-.171	.136	-.049	.116	-.283**	.405**	.375**	**.632****	**.741****	1												
Cd	.016	.294**	.210*	.282**	.255**	.224*	.142	.262**	.219*	-.139	.090	-.061	.106	-.295**	.258**	.325**	**.874****	**.878****	**.743****	1											
Cr	-.095	.175	.000	.153	.173	.173	.073	.165	.162	.137	.027	-.133	.089	.028	.165	.056	.365**	.288**	.236*	.348**	1										
Cu	.106	**.858****	.422**	**.788****	**.844****	**.782****	**.512****	**.840****	.405**	-.256**	**.637****	-.146	.210*	-.566**	**.846****	**.684****	**.644****	**.518****	.428**	.436**	.232*	1									
Hg	.229*	-.025	-.008	-.033	-.023	-.035	-.048	-.021	-.079	-.143	-.054	-.067	.098	-.128	-.025	.136	.013	.006	.106	.066	-.077	.000	1								
Ni	-.210*	.483**	**.700****	**.538****	.408**	.330**	.308**	.446**	.003	-.105	.409**	-.142	.015	-.212*	.448**	**.502****	**.601****	**.790****	**.705****	**.720****	.184*	.471**	.076	1							
Pb	.127	-.056	-.037	-.053	-.053	-.065	-.008	-.052	.107	-.073	-.066	-.051	.076	-.096	-.054	-.031	-.039	-.030	.004	-.007	-.007	.006	-.009	-.015	1						
Sb	.042	.333**	.223*	.386**	.275**	.265**	.088	.297**	.124	-.154	.071	-.072	.107	-.273**	.288**	.272**	.739**	.429**	.371**	**.657****	.276**	.396**	.032	.440**	-.017	1					
MI	.029	**.552****	.376**	**.512****	**.516****	.466**	.333**	**.522****	.340**	-.175	.362**	-.139	.121	-.383**	**.524****	**.516****	**.721****	**.815****	**.700****	**.748****	.305**	**.601****	.005	**.745****	.469**	.443**	1				
HPI	.022	**.977****	.488**	**.876****	**.970****	**.980****	**.531****	**.978****	.334**	-.150	**.598****	-.140	.182	-.523**	**.976****	**.659****	.494**	.400**	.448**	.296**	.177	**.834****	.035	.438**	.031	.322**	**.579****	1			
GWQI	-.004	**.996****	**.536****	**.894****	**.994****	**.960****	**.557****	**.998****	.323**	-.154	**.663****	-.140	.161	-.500**	**.999****	**.664****	.485**	.409**	.432**	.287**	.173	**.851****	-.016	.469**	-.032	.305**	**.556****	**.983****	1		
Se	-.103	**.741****	**.512****	**.692****	**.702****	**.666****	.416**	**.717****	.278**	-.108	.463**	-.113	.076	-.357**	**.716****	**.582****	**.754****	**.868****	**.783****	**.761****	.293**	**.687****	-.009	**.842****	-.054	.447**	**.836****	**.726****	**.737****	1	
Zn	.131	**.584****	.468**	.490**	**.571****	.484**	.414**	**.573****	.254**	-.250**	.443**	-.140	.197*	-.436**	**.577****	**.524****	.491**	**.526****	.490**	.477**	.182	**.620****	.039	**.561****	.459**	.264**	**.790****	**.587****	**.593****	**.640****	1

** Correlation is significant at the 0.01 level (2-tailed).
* Correlation is significant at the 0.05 level (2-tailed).

Table 4
Principal component loadings and explained variance of the analyzed parameters with varimax normalized rotation.

	Component						
	1	2	3	4	5	6	7
pH	−0.030	−0.031	0.760	0.062	0.175	0.093	0.298
EC	0.962	0.235	0.013	0.090	0.057	0.020	−0.015
Ca^{2+}	0.477	0.247	−0.559	0.423	0.156	0.077	0.137
Mg^{2+}	0.859	0.266	−0.137	0.138	0.101	−0.008	0.027
Na^{+}	0.968	0.180	0.065	0.045	0.037	0.026	−0.028
K^{+}	0.956	0.142	0.063	−0.086	0.035	0.002	−0.018
NH_4^{+}	0.542	0.082	0.019	0.435	0.076	0.045	−0.209
Cl^{-}	0.972	0.193	−0.004	0.035	0.046	0.031	0.002
HCO_3^{-}	0.267	0.199	0.766	0.095	0.053	0.061	−0.244
NO_3^{-}	−0.061	−0.113	−0.447	−0.545	−0.399	−0.009	−0.189
SO_4^{2-}	0.631	0.075	0.025	0.590	0.078	−0.017	−0.176
NO_2^{-}	−0.076	−0.045	0.045	−0.110	−0.846	−0.023	0.061
PO_4^{3-}	0.121	0.035	0.245	−0.048	0.774	0.064	0.150
SiO_2	−0.487	−0.210	−0.367	−0.080	−0.061	−0.134	−0.393
TDS	0.972	0.190	0.008	0.068	0.050	0.028	−0.015
F^{-}	0.612	0.318	0.087	0.440	−0.013	0.025	0.151
As	0.318	0.847	0.271	−0.081	0.041	−0.047	−0.022
B	0.194	0.894	0.103	0.214	−0.009	0.043	−0.111
Ba	0.253	0.778	−0.065	0.070	0.015	0.089	0.109
Cd	0.074	0.966	0.070	−0.037	0.024	0.026	0.027
Cr	0.125	0.383	−0.015	−0.442	0.255	−0.003	−0.417
Cu	0.798	0.366	0.188	0.109	0.082	0.054	−0.012
Hg	−0.032	0.067	0.021	−0.013	0.087	−0.018	0.779
Ni	0.279	0.777	−0.368	0.314	0.044	0.092	0.050
Pb	−0.071	−0.033	0.091	−0.053	0.045	0.954	−0.001
Sb	0.198	0.645	0.062	−0.226	0.117	−0.117	0.138
MI	0.367	0.740	0.043	0.096	0.032	0.527	−0.070
HPI	0.954	0.225	0.040	−0.004	0.054	0.096	0.044
GWQI	0.966	0.220	0.009	0.061	0.049	0.049	−0.009
Se	0.566	0.762	−0.092	0.118	−0.013	0.061	−0.074
Zn	0.468	0.428	0.039	0.201	0.097	0.615	0.035
% of Variance	45.00	11.49	8.06	5.26	4.62	4.09	3.64
Cumulative %	45.00	56.48	64.55	69.81	74.43	78.52	82.17

area. The NE–SW fault system facelifted seawater intrusion into the groundwater and for groundwater discharge to the Red Sea.

CRediT authorship contribution statement

Authors	Field trip and collecting sediments	Preparing sediments for analysis	Interpretation of chemical analysis	Manuscript writing	Manuscript submission
Fahad Alshehri	√	√	√	√	
Sattam Almadani		√	√	√	
Abdelbaset El-Sorogy		√	√	√	√
Essam Alwaqdani	√	√	√	√	
Hussain J. Alfaifi		√	√	√	
Talal Alharbi		√	√	√	

Declaration of competing interest

The authors declare that they have no known competing financial interests or personal relationships that could have appeared to influence the work reported in this paper.

Acknowledgements

The authors extend their appreciation to the Deputyship for Research & Innovation, “Ministry of Education” in Saudi Arabia for funding this research work through the project number IFKSURG-1442-117.

Appendix A. Supplementary data

Supplementary data to this article can be found online at https://doi.org/10.1016/j.marpolbul.2021.112094.

References

Abdelkareem, M., Bamousa, A.O., Hamimi, Z., Kamal, El-Din, G.M., 2020. Multispectral and RADAR images integration for geologic, geomorphic, and structural investigation in southwestern Arabian Shield, Al Qunfudhah area, Saudi Arabia. Journal of Taibah University for Science 14 (1), 383–401.

Abu Jabal, M.S., Abustan, I., Rozainy, Z.M.R., Al-Najar, H., 2014. Groundwater beneath the urban area of Khan Younis City, southern Gaza Strip (Palestine): hydrochemistry and water quality. Arab. J. Geosci. 8 (4) https://doi.org/10.1007/s12517-014-1346-6.

Alfaifi, H., El-Sorogy, A.S., Qaysi, S., Kahal, A., Almadani, S., Alshehri, F., Zaidi, F.K., 2021. Evaluation of heavy metal contamination and groundwater quality along the Red Sea coast, southern Saudi Arabia. Mar. Poll. Bull. https://doi.org/10.1016/j.marpolbul.2021.111975.

Alshehri, F., Sultan, M., Karki, S., Alwagdani, E., Alsefry, S., Alharbi, H., Sahour, H., Sturchio, N., 2020. Mapping the distribution of shallow groundwater occurrences using remote sensing-based statistical modeling over southwest Saudi Arabia. Remote Sens. 12, 1361.

Aswathanarayana, U., Lahermo, P., Malisa, E., Nanyaro, J.T., 1985. High fluoride waters in an endemic fluorosis area in northern Tanzania. In: Thornton, I. (Ed.), Proceedings of the 1st International Symposium on Geochemistry and Health Monograph Series: Environmental Geochemistry and Health, pp. 243–249.

Backman, B., Bodis, D., Lahermo, P., Rapant, S., Tarvainen, T., 1997. Application of a groundwater contamination index in Finland and Slovakia. Environ. Geol. 36, 55–64.

Baghvand, A., Nasrabadi, T., Bidhendi, G.N., Vosoogh, A., Karbassi, A., Mehrdadi, N., 2010. Groundwater quality degradation of an aquifer in Iran central desert. Desalination 260, 264–275.
Basahi, J.M., Masoud, M.H.Z., Rajmohan, N., 2018. Effect of flash flood on trace metal pollution in the groundwater - Wadi Baysh Basin, western Saudi Arabia. J. Afr. Earth Sci. 147, 338–351.
Bayumi, T., Alyamani, M., Subyani, M.S., Al-Ahmadi, M., 2000. Analytical study of flood problems and groundwater rise in the Jeddah District. Final Rep. Proj. 606, 418.
Bodrud-Dozaa, M.D., Islam, A.R.M., Ahmed, F., Das, S., Saha, N., Rahman, M.S., 2016. Characterization of groundwater quality using water evaluation indices, multivariate statistics and geostatistics in central Bangladesh. Water Sc. 30, 19–40.
Caerio, S., Costa, M.H., Ramos, T.B., Fernandes, F., Silveira, N., Coimbra, A., Painho, M., 2005. Assessing heavy metal contamination in Sado estuary sediment: an index analysis approach. Ecol. Indic 5, 155–169.
Chiamsathit, C., Auttamana, S., Thammarakcharoen, S., 2020. Heavy metal pollution index for assessment of seasonal groundwater supply quality in hillside area, Kalasin, Thailand. Appl. Water Sci. 10, 142.
Cloutier, V., Lefebvre, R., Therrien, R., et al., 2008. Multivariate statistical analysis of geochemical data as indicative of the hydrogeochemical evolution of groundwater in a sedimentary rock aquifer system. J. Hydrol. 353, 294–313.
Dissanayake, C.B., Chandrajith, R., 2009. Introduction to Medical Geology, Focus on Tropical Environments. Springer-Verlag, Berlin Heidelberg, 297 pp.
Enaam Abdullah, J., 2013. Quality assessment for Shatt Al-Arab River using heavy metal pollution index and metal index. J. Environ. Earth Sci. 3, 114.
Evanko, F.R., Dzombak, D.A., 1997. Remediation of metals contaminated soils and groundwater. In: Tech. Rep. TE-97-01, Groundwater Remediation Technologies Analysis Centre, Pittsburg, PA, USA.
Kampouroglou, E.E., Economou-Eliopoulos, M., 2017. Assessment of arsenic and associated metals in the soil-plant-water system in Neogene basins of Attica, Greece. Catena 150, 206–222.
Kumar, P.J.S., 2014. Evolution of groundwater chemistry in and around Vaniyambadi Industrial Area: differentiating the natural and anthropogenic sources of contamination. Geochemistry 74 (4), 641–651.
Li, P., Wu, J., Qian, H., 2016. Hydrochemical appraisal of groundwater quality for drinking and irrigation purposes and the major influencing factors: a case study in and around Hua County, China. Arab. J. Geosci. 9, 15.
Li, P., He, X., Li, Y., et al., 2018. Occurrence and health implication of fluoride in groundwater of loess aquifers in the Chinese Loess Plateau: A case study of Tongchuan, northwest China. Expo. Health. https://doi.org/10.1007/s12403-018-0278-x.
Lu, S.G., Tang, C., Rengel, Z., 2004. Combined effects of waterlogging and salinity on electrochemistry, water-soluble cations and water dispersible clay in soils with various salinity levels. Plant Soil 264, 231–245.
Lyulko, T., Ambalova, T., Vasiljeva, T., 2001. To integrated water quality assessment in Latvia, MTM (monitoring tailor-made) III. In: Proceedings of international workshop on information for sustainable water management, Netherlands, pp. 449–452.
Mohan, S.V., Nithila, P., Reddy, S.J., 1996. Estimation of heavy metal in drinking water and development of heavy metal pollution index. J. Environ. Sci. Health A31, 283–289.
Nabizadeh, R., Valadi Amin, M., Alimohammadi, M., Naddafi, K., Mahvi, A.H., Yousefzadeh, S., 2013. Development of innovative computer software to facilitatethe setup and computation of water quality index. J. Environ. Health Sci. Eng. 11, 1.
Naidu, R., Bhattacharya, P., 2009. Arsenic in the environment—risks and management strategies. Environ. Geochem. Health 1, 1–8.
Panigrahy, B.P., Singh, P.K., Tiwari, A.K., Kumar, B., Kumar, A., 2015. Assessment of heavy metal pollution index for groundwater around Jharia coalfield region, India. J. Biodivers. Environ. Sci. 6, 33–39.
Prasad, B., Sangita, K., 2008. Heavy metal pollution index of groundwater of an abandoned open cast mine filled with fly ash: a case study. Mine Water Environ. 27, 265–267.
Prasanna, M.V., Chitambaram, S., Hameed, A.S., Srinivasamoorthy, K., 2011. Hydrogeochemical analysis and evaluation of groundwater quality in the Gadilam river basin, Tamil Nadu, India. J. Earth Syst. Sci. 120 (1), 85–98.
Prinz, W.C., 1983. Geologic Map of the Al Qunfudhah Quadrangle, Sheet 19 E, Kingdom of Saudi Arabia. Ministry of petroleum and Mineral Resources, Saudi Arabia.
Prinz, C., 1984. Geology Map of the Wadi Haliy Quadrangle, Sheet 18E, Kingdom of Saudi Arabia, Ministry of Petroleum and Mineral Resources Deputy Ministry for Mineral Resources. U.S. Geol. Surv., Saudi Arabia Mission.
Rahman, M.A.T.M.T., Saadat, A.H.M., Islam, M.S., Al-Mansu, M.A., Ahmed, S., 2014. Groundwater characterization and selection of suitable water type for irrigation in the western region of Bangladesh. Appl Water Sci. https://doi.org/10.1007/s13201-014-0239-x.
Ramakrishnaiah, C.R., Sadashivaiah, C., Ranganna, G., 2009. Assessment of water quality index for the groundwater in Tumkur Taluk, Karnataka State, India. E-J. Chemi. 6 (2), 523–530.
Rezaei, A., Hassani, H., Hassani, S., Jabbari, N., Mousavi, S.B.F., Rezaei, S., 2019a. Evaluation of groundwater quality and heavy metal pollution indices in Bazman basin, southeastern Iran. Groundwater Sustain Dev 9, 100245.
Rezaei, A., Hassani, H., Jabbari, N., 2019b. Evaluation of groundwater quality and assessment of pollution indices for heavy metals in North of Isfahan Province, Iran. Sustain Water Resour. Manag. 5, 491–512.
Rizwan, R., Gurdeep, S., Manish Kumar, J., 2011. Application of heavy metal pollution index for ground water quality assessment in Angul district of Orissa, India. Int. J. Res. Chem. Environ. 1, 118–122.
Sahour, H., Vazifedan, M., Alshehri, F., 2020a. Aridity trends in the Middle East and adjacent areas. Theor. Appl. Climatol. 142 (3), 1039–1054.
Sahour, H., Gholami, V., Vazifedan, M., 2020b. A comparative analysis of statistical and machine learning techniques for mapping the spatial distribution of groundwater salinity in a coastal aquifer. J. Hydrol. 591, 125321.
Sahu, P., Sikdar, P.K., 2008. Hydrochemical framework of the aquifer in and around East Kolkata Wetlands, West Bengal, India. Environ. Geol. 55, 823–835.
Sharma, N.D., Patel, J.N., 2010. Evaluation of Groundwater Quality Index of the Urban Segments of Surat City, India. International Journal of Geology 1 (4), 1–4.
Sheykhi, V., Moore, F., 2012. Geochemical characterization of Kor River water quality, Fars Province, Southwest Iran. Water Qual. Expo. Health. 4, 25–38.
Singaraja, C., Chidambaram, S., Prasanna, M.V., Thivya, C., Thilagavathi, R., 2014. Statistical analysis of the hydrogeochemical evolution of groundwater in hard rock coastal aquifers of Thoothukudi district in Tamil Nadu, India. Environ. Earth Sci. 71, 451–464.
Sirajudeen, J., Arul, Manikandan, S., Manivel, V., 2014. Heavy metal pollution index of ground water of Fathima Nagar area near Uyyakondan Channel, Tiruchirapalli District, Tamil Nadu, India. World J. Pharm. Pharm. Sci. 4, 967–975.
Sulaiman, A., Elawadi, E., Mogren, S., 2018. Gravity interpretation to image the geologic structures of the coastal zone in al Qunfudhah area, southwest Saudi Arabia. Geophys. J. Int. 214, 1623–1632.
Sultan, M., Chamberlain, K.R., Bowring, S.A., Arvidson, R.E., Abuzied, H., El Kaliouby, B., 1990. Geochronologic and isotopic evidence for involvement of pre-Pan-African crust in the Nubian Shield, Egypt. Geology 18, 761–764.
Tamasi, G., Cini, R., 2004. Heavy metals in drinking waters from Mount Amiata (Tuscany, Italy). Possible risks from arsenic for public health in the province of Siena. Sci. Total Environ 327, 41–51.
Vasanthavigar, M., Srinivasamoorthy, K., Vijayaragavan, K., Ganthi, R.R., Chidambaram, S., Anandhan, P., Manivannan, R., Vasudevan, S., 2010. Application of water quality index for groundwater quality assessment: Thirumanimuttur sub-basin Tamilnadu, India. Environ. Monit. Assess. 171, 595–609.
Wang, S., Mulligan, C.N., 2006a. Occurrence of arsenic contamination in Canada: sources, behavior and distribution. Sci. Total Environ. 366, 701–721.
Wang, S., Mulligan, C.N., 2006b. Effect of natural organic matter on arsenic release from soils and sediments into groundwater. Environ. Geochem. Health 28, 197–214.
Wen, X., Lub, J., Wu, J., Lin, Y., Luo, Y., 2019. Influence of coastal groundwater salinization on the distribution and risks of heavy metals. Sci. Total Environ. 652, 267–277.
WHO (Ed.), 2004. Guidelines for Drinking-water Quality, 3rd ed. WHO, Geneva, Switzerland.
WHO, 2011. Guidelines for Drinking Water Quality, 4th ed. Geneva, Switzerland.
Wu, J., Li, P., Wang, W., Ren, X., Wei, M., 2020. Statistical and multivariate statistical techniques to trace the sources and affecting factors of groundwater pollution in a rapidly growing city on the Chinese Loess Plateau. Hum. Ecol. Risk. Assess. 26 (6), 1603–1621.